TES OBSERVATIONS OF AEROSOL OPTICAL DEPTH AND WATER VAPOR ABUNDANCE

M. D. Smith[1], B. J. Conrath[2], J. C. Pearl[1], and P. R. Christensen[3],
[1]NASA Goddard Space Flight Center, Greenbelt, MD 20771 USA (Michael.D.Smith.1@gsfc.nasa.gov), [2]Cornell University, Ithaca, NY 14853 USA, [3]Arizona State University, Tempe, AZ 85287 USA.

Introduction: Spectra from the Mars Global Surveyor (MGS) Thermal Emission Spectrometer (TES) have been used to monitor the latitude, longitude, and seasonal dependence of dust and water ice aerosols and water vapor for nearly two full Martian years. A brief description of the TES instrument [*Christensen et al.,* 2001] and the thermal structure of the Martian atmosphere as observed by TES is given in an accompanying abstract.

Dust Aerosols: Dust aerosols are always present in the Mars atmosphere. Their presence significantly affects the thermal structure of the atmosphere and is a major driver of atmospheric circulations at all spatial scales. The retrieval algorithm for dust optical depth from TES spectra is given by *Smith et al.* [2000].

Figure 1 shows the seasonal and latitudinal dependence of dust optical depth as observed by TES. The dust activity shown in the top panel of Fig. 1 represents a Martian year with only moderate dust storm activity. No planet-encircling dust storms were observed. Average IR dust optical depth was comparable with that during comparable seasons of the previous Martian year observed by TES during aerobraking (1997-1998) [*Smith et al.,* 2000], but substantially less than that observed during the second MGS mapping year (middle panel of Fig. 1), or by Mariner 9 [*Fenton et al.,* 1997] or during the first Viking year [*Martin and Richardson,* 1993].

During the first MGS mapping year (top panel, Fig. 1), the largest dust storm activity (Ls=225°-245°) was the result of two principal storm centers. Both had IR optical depth reaching unity in their respective cores, but neither attained global status. A strong but smaller regional dust storm began poleward of 70° S latitude just before Ls=260° but it did not spread northward. Other regional dust storms during the periods Ls=170°-190° and Ls=320°-350° reached only moderate IR optical depth (~0.4). The period Ls=30°-130° had the lowest globally-averaged optical depth.

During the second MGS mapping year (middle panel, Fig. 1), the initiation, evolution, and decay of a planet-encircling dust storm was observed [*Smith et al.,* 2002]. A local dust storm near Hellas began to rapidly expand on 26 June 2001 (Ls=185°) becoming a planet-encircling dust storm by 11 July 2001 (Ls=193°). This is the earliest seasonal date ever observed for a planet-encircling dust storm. The dust storm had 9-μm dust optical depth of ~2 over wide areas and caused atmospheric temperatures over a large vertical range to warm by > 40 K from 20° N latitude to the south pole. The amplitude of the Hadley circulation and thermal tides were enhanced. Dust optical depth and atmospheric temperatures reached their maximum values around 1 August 2001 (Ls=206°). The subsequent clearing of the dust storm was more rapid at high southerly latitudes than near the equator.

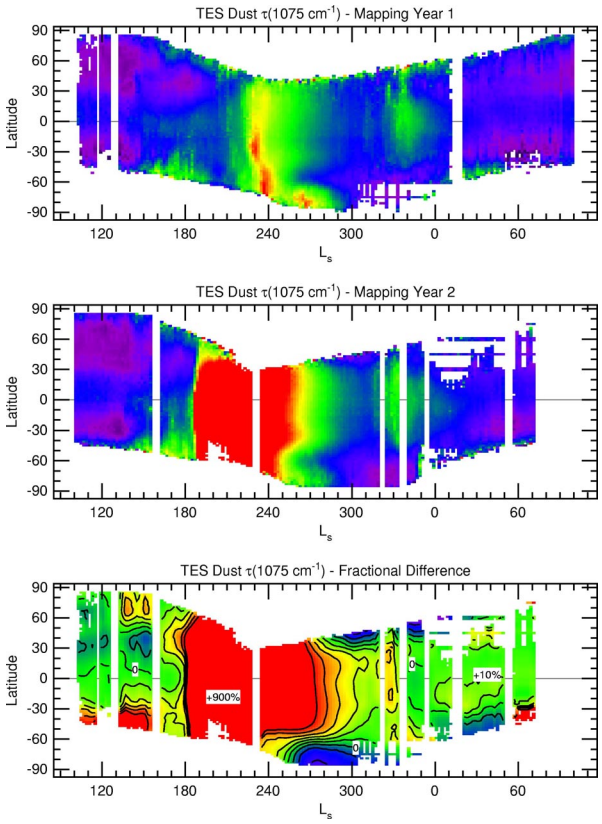

Figure 1. The daytime dust optical depth (1075 cm^{-1}, scaled to an equivalent 6.1-mbar pressure level), as a function of season and latitude. Scale for optical depth is from zero (purple) to >0.5 (red). (top) First MGS mapping year (1999-2000), (middle) second mapping year (2001-2002), (bottom) fractional difference from year one to year two. Scale for the fractional difference is from +50% (red) to no change (green) to –50%

(purple) with contours every 10%.

The bottom panel of Fig. 1 shows the fractional difference in dust optical depth from MGS mapping year one to year two. It is dominated by the presence of the planet-encircling storm in the second mapping year. However, other similarities and differences between the two years are notable. Moderate dust activity beginning around Ls=140°-150° along the edge of the receding south polar cap is prominent during both years. A regional dust storm at Ls=320°-350° at low latitudes occurred during both years (and during the previous Martian year in the aerobraking period too [*Smith et al.,* 2000]). Notable differences (besides the planet-encircling dust storm) include the absence in the second year of the concentration of dust activity at Ls=270° at high southerly latitudes (which was also observed during aerobraking). Outside of the seasons and latitudes affected by dust storms, the "nominal" dust loading was consistent to within about 20% between the two years (generally somewhat higher during the second year).

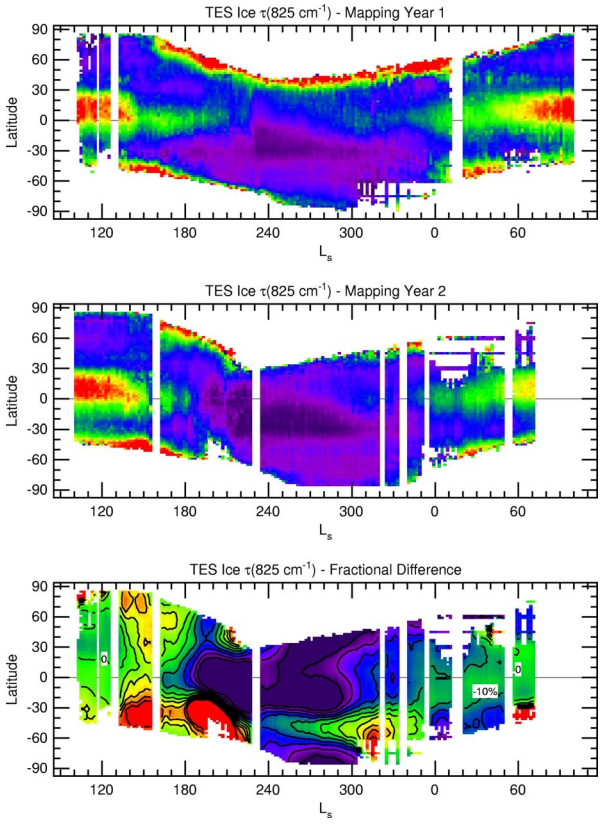

Figure 2. The daytime water-ice optical depth (825 cm^{-1}, NOT scaled to an equivalent 6.1-mbar pressure surface), as a function of season and latitude. Scale for optical depth is from zero (purple) to >0.15 (red). (top) First MGS mapping year (1999-2000), (middle) second mapping year (2001-2002), (bottom) fractional difference from year one to year two. Scale for the fractional difference is from +50% (red) to no change (green) to –50% (purple) with contours every 10%.

Water-Ice Aerosols: Water-ice aerosols in the form of clouds and fogs are now known to be an important part of the present-day climate system on Mars. More background about water-ice clouds on Mars and a detailed description of the retrieval algorithm used by TES is given by *Pearl et al.* [2001].

Figure 2 shows the seasonal and latitudinal dependence of water ice cloud optical depth as observed by TES. The most striking feature is the low-latitude belt of clouds that extends from 10° S to 30° N latitude from Ls=40°-145°. This aphelion-season cloud belt was prominent at all longitudes with enhancements over regions of high topography such as Tharsis and Elysium. Similar aphelion-season water-ice cloud belts have been observed in previous years (e.g. [*Clancy et al.,* 1996]).. The column-integrated water content in these clouds is typically a couple pr-µm. The cloud optical depth decreased abruptly at Ls=145° during both the first MGS mapping year (top panel of Fig. 2) and the second MGS mapping year (middle panel of Fig. 2), although a maximum in zonally-averaged water-ice optical depth at low latitudes persisted throughout the year because of the Olympus Mons, Tharsis, and Elysium topographic features. Beginning at Ls=160°, the formation of the polar hood was seen at mid-northerly latitudes at the edge of the results shown in Fig. 2. A weaker, less extensive polar hood was observed I the south during southern winter. The temperature increase associated with planet-encircling and large regional dust storms effectively removes all water ice clouds from the atmosphere.

The bottom panel of Fig. 2 shows the fractional difference in water-ice optical depth from MGS mapping year one to year two. Although there is a lot of structure in the figure, much of high fractional differences occur when the ice optical depth is low so that the absolute difference in optical depth units is small. The planet-encircling dust storm cut off the "tail" of moderate low-latitude ice opacity after Ls=185°, although it is interesting to note that those clouds were somewhat less extensive even before the start of the 2001 dust storm (i.e. from Ls=170°-185°). On the other hand, there was somewhat higher ice cloud optical depth during the second mapping year throughout southern hemisphere summer at the edge of the southern ice cap. The planet-encircling dust storm during the second MGS mapping year either greatly reduced the northern polar hood clouds or else shifted them northward to a latitude where the retrieval breaks down from insufficient thermal contrast. Perhaps the largest difference is

the relatively slow regeneration of the current (2002-2003) aphelion-season ice belt. Throughout the initial stages of its growth between Ls=0° and 60°, the aphelion-season cloud belt has had noticeably less optical depth this year (by 10-20%) as compared with the first MGS mapping year. As of about Ls=60° most of this deficit was made up so that the 2002 and 2000 cloud belts were of comparable optical depth.

Water Vapor: Although water vapor is a minor constituent in the atmosphere of Mars, it still plays an important role. Along with the annual cycles of CO_2 and dust, the annual cycle of water is one of the three main cycles that define the present Martian climate. A detailed description of the retrieval algorithm used for water vapor and a comparison of these values with Viking and other observations of water vapor is given by *Smith* [2002].

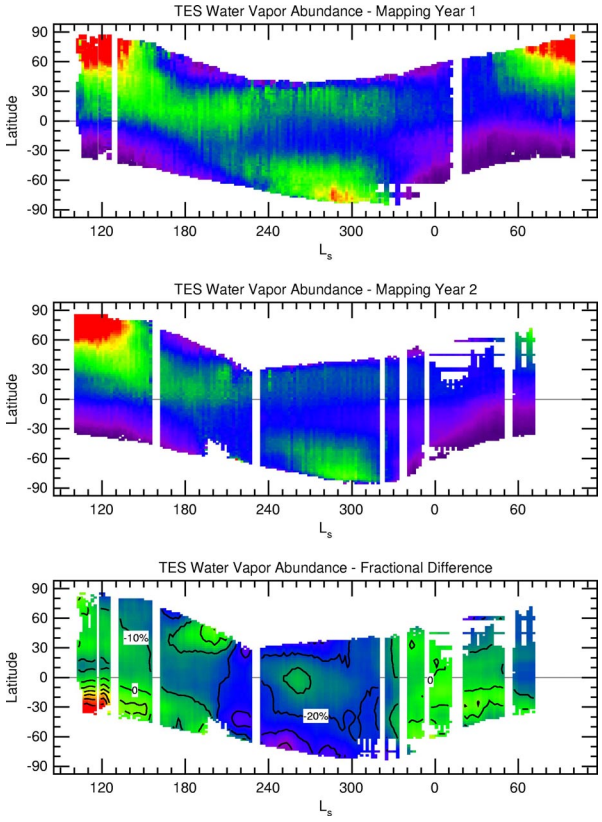

Figure 3. The daytime water vapor column abundance, (NOT scaled to an equivalent 6.1-mbar pressure surface), as a function of season and latitude. Scale for vapor abundance is from zero (purple) to >50 pr-µm (red). (top) First MGS mapping year (1999-2000), (middle) second mapping year (2001-2002), (bottom) fractional difference from year one to year two. Scale for the fractional difference is from +50% (red) to no change (green) to –50% (purple) with contours every 10%.

Figure 3 shows the seasonal and latitudinal dependence of water vapor abundance as observed by TES. A maximum in water vapor abundance is observed at high latitudes during mid-summer in both hemispheres, reaching a maximum value of ~100 pr-µm in the north and as high as 50 pr-µm in the south. Low water vapor abundance (<5 pr-µm) is observed at middle and high latitudes in the fall and winter of both hemispheres. There are large differences in the hemispheric (north versus south) and seasonal (perihelion versus aphelion) behavior of water vapor. The latitudinal and seasonal dependence of the decay of the northern summer water vapor maximum implies cross-equatorial transport of water to the southern hemisphere, while there is little or no corresponding transport during the decay of the southern hemisphere summer maximum. A very steep latitudinal gradient in water vapor abundance (high in the north) forms during early northern summer (Ls=90·-150°), while water vapor is distributed more uniformly in latitude during early southern summer (Ls=270°-330°). The annually-averaged amount of water vapor in the Martian atmosphere is 17 pr-µm in the northern hemisphere and 9.5 pr-µm in the southern hemisphere (for the first MGS mapping year). However, when referenced to a 6.1-mbar equivalent pressure surface to remove the effect of topography, the annually-averaged amount of water vapor becomes 17 pr-µm in the latitude band from 10° S to 40° N, and 12 pr-µm everywhere else. The latitude-longitude dependence of annually-averaged water vapor (corrected for topography) has a significant positive correlation with albedo and significant negative correlations with thermal inertia and surface pressure. Comparison of TES results with those retrieved form the Viking Orbiter Mars Atmospheric Water Detectors (MAWD) experiments [*Jakosky and Farmer*, 1982] shoes some similar features, but also many significant differences. The southern hemisphere maximum observed by TES was not observed by MAWD and the large latitudinal gradient in annually-averaged water vapor observed by MAWD does not appear in the TES results.

Although the season-latitude dependence of water vapor is similar for the first two MGS mapping years (top panel of Fig. 3 shows 1999-2000, middle panel shows 2001-2002), there are some significant differences between the two years. The bottom panel of Fig. 3 shows the fractional difference in water vapor abundance from MGS mapping year one to year two. Water vapor abundance has been lower during the second MGS mapping year than during the first year for almost all seasons and latitudes. Typically the difference has been about 10%, although the most recent (2002) southern hemisphere summer maximum had water vapor column abundance roughly 25% lower than the

previous year. We do not believe that a bias in the retrievals caused by the planet-encircling dust storm of 2001 is the cause of this difference. Water vapor abundance was already down by more than 10% compared to the previous year well before the beginning of the dust storm at Ls=185°. Furthermore, there was significant clearing from the dust storm (see Fig. 1) by Ls=300°, especially at high southerly latitudes, but this is one of the seasons and latitudes that is most deficient in water vapor this past year. Water vapor levels were similar for the two years at the annual minimum of water vapor at about Ls=0°-30°, but since that time the northern springtime increase water vapor abundance has progressed at a slower rate this year. It will be very interesting to see whether or not the northern summer maximum attains the 100 pr-μm level that it has the previous two Martian years (and during Viking).

Summary: TES spectra allow detailed monitoring of the seasonal and spatial distribution of dust and water ice aerosols and water vapor abundance. The extended life of the MGS mission allows the determination of the amount of interannual variability in atmospheric quantities using a consistent dataset from a single instrument. These data are useful both for the characterization of the present Martian climate state as well as for serving as the "ground-truth" against which modeling results can be tested.

References:

Christensen et al., 2001, *Icarus 122*, 36.
Clancy et al., 1996, *J. Geophys. Res. 105*, 9553.
Conrath et al., 2000, *J. Geophys. Res. 105*, 9509.
Fenton et al., 1997, *Icarus 130*, 115.
Jakosky and Farmer, 1982, *J. Geophys. Res. 87*, 2999.
Martin and Richardson, 1993, *J. Geophys. Res. 98*, 10,941.
Pearl et al., 2001, *J. Geophys. Res. 106*, 12,325.
Pollack et al., 1977, *J. Geophys. Res. 82*, 4479.
Smith et al., 1997, *Science 278*, 1758.
Smith et al., 2000, *J. Geophys. Res. 105*, 9539.
Smith et al., 2001, *J. Geophys. Res. 106*, 23,929.
Smith et al., 2002, *Icarus 157*, 259.
Smith 2002. The annual cycle of water vapor on Mars as observed by the Thermal Emission Spectrometer, *J. Geophys. Res.,* in press